

Restoring Sparsity in Potts Machines via Mean-Field Constraints

Kevin Callahan-Coray,¹ Kyle Lee,¹ Kyle Jiang,¹ and Kerem Y. Çamsarı¹

¹*Department of Electrical and Computer Engineering,
University of California, Santa Barbara, Santa Barbara, CA 93106, USA*

(Dated: February 5, 2026)

Ising machines and related probabilistic hardware have emerged as promising platforms for NP-hard optimization and sampling. However, many practical problems involve constraints that induce dense or all-to-all couplings, undermining scalability and hardware efficiency. We address this constraint-induced density through two complementary approaches. First, we introduce a hardware-aware native formulation for multi-state probabilistic digits (p-dits) that avoids the locally dense intra-variable couplings required by binary Ising encodings. We validate p-bit dynamics by reproducing known critical behavior of the 2D Potts model. Second, we propose mean-field constraints (MFC), a hybrid scheme that replaces dense pairwise constraint couplings with dynamically updated single-node biases. Applied to balanced graph partitioning, MFC achieves solution quality comparable to exact all-to-all constraint formulations while dramatically reducing graph density. Finally, we demonstrate the practical impact of restored sparsity by an FPGA implementation, enabling orders-of-magnitude acceleration over CPU-based solvers. Together, these results outline a pathway for scaling constrained optimization on probabilistic hardware.

I. INTRODUCTION

Ising machines and related probabilistic computing architectures have emerged as promising platforms not only for accelerating NP-hard optimization but also for sampling tasks relevant to machine learning and as components in hybrid classical-quantum workflows [1–3]. A key factor underlying their reported scalability is the sparsity of the interaction graph, which enables localized updates, low communication overhead, and efficient implementation across digital [4, 5], analog [6], and mixed-signal [7] hardware platforms. As a result, much of the existing work on Ising machines has focused on unconstrained or weakly constrained optimization problems, where sparsity is preserved and large systems can be simulated or realized efficiently [4].

In contrast, many relevant optimization problems are dominated by constraints that fundamentally alter this sparsity structure. Constraints such as balancing, cardinality, exclusivity, and resource conservation often introduce dense or all-to-all interactions, even when the underlying objective function is sparse [8]. Enforcing such constraints through penalty terms or auxiliary variables leads to interaction graphs whose density scales poorly with problem size [5], eroding parallelism and substantially increasing computational and hardware cost. As a result, constraint enforcement emerges as a primary obstacle to scaling Ising machines for real-world applications.

This work addresses constraint-induced density by introducing two complementary mechanisms that restore sparsity in constrained probabilistic optimization. First, we propose a hardware efficient probabilistic digit (p-bit) [9], a multi-state generalization of probabilistic bits (p-bits) [10] that absorbs local constraints directly into the node state space. By embedding mutually exclusive configurations into a single multi-state variable, p-dits eliminate dense intra-variable penalty couplings

while preserving the exact local energy structure. Second, we introduce mean-field constraints (MFC), a hybrid probabilistic-classical approach in which global constraints are enforced approximately through dynamically updated bias signals. This decouples global constraint enforcement from local stochastic updates, replacing dense pairwise interactions with a shared, slowly varying mean field.

We demonstrate the effectiveness of these approaches using the balanced graph partitioning problem, a canonical example of constrained optimization that combines a sparse objective with a global balancing constraint. Using this problem as a test case, we show that mean-field constraints achieve solution quality comparable to strictly constrained formulations while dramatically reducing effective graph density. Finally, we validate the practical impact of restored sparsity through an FPGA implementation, demonstrating that constrained optimization problems can recover the parallelism and performance associated with sparse Ising machines when constraint-induced density is removed.

II. MULTI-STATE PROBABILISTIC DIGITS (P-DITS)

The Potts model generalizes the Ising model, where binary spins $m_i \in \{-1, +1\}$ evolve to minimize $E = -\sum_{i < j} J_{ij} m_i m_j - \sum_i h_i m_i$, by allowing each variable to occupy one of Q discrete states, $s_i \in \{0, 1, \dots, Q-1\}$ [14]. The most general first-order Potts Hamiltonian is

$$E = - \sum_{i < j} J_{ij}(s_i, s_j) - \sum_i h_i(s_i), \quad (1)$$

where $J_{ij}(s_i, s_j)$ defines the interaction energy between states of nodes i and j , and $h_i(s_i)$ is a state-dependent bias.

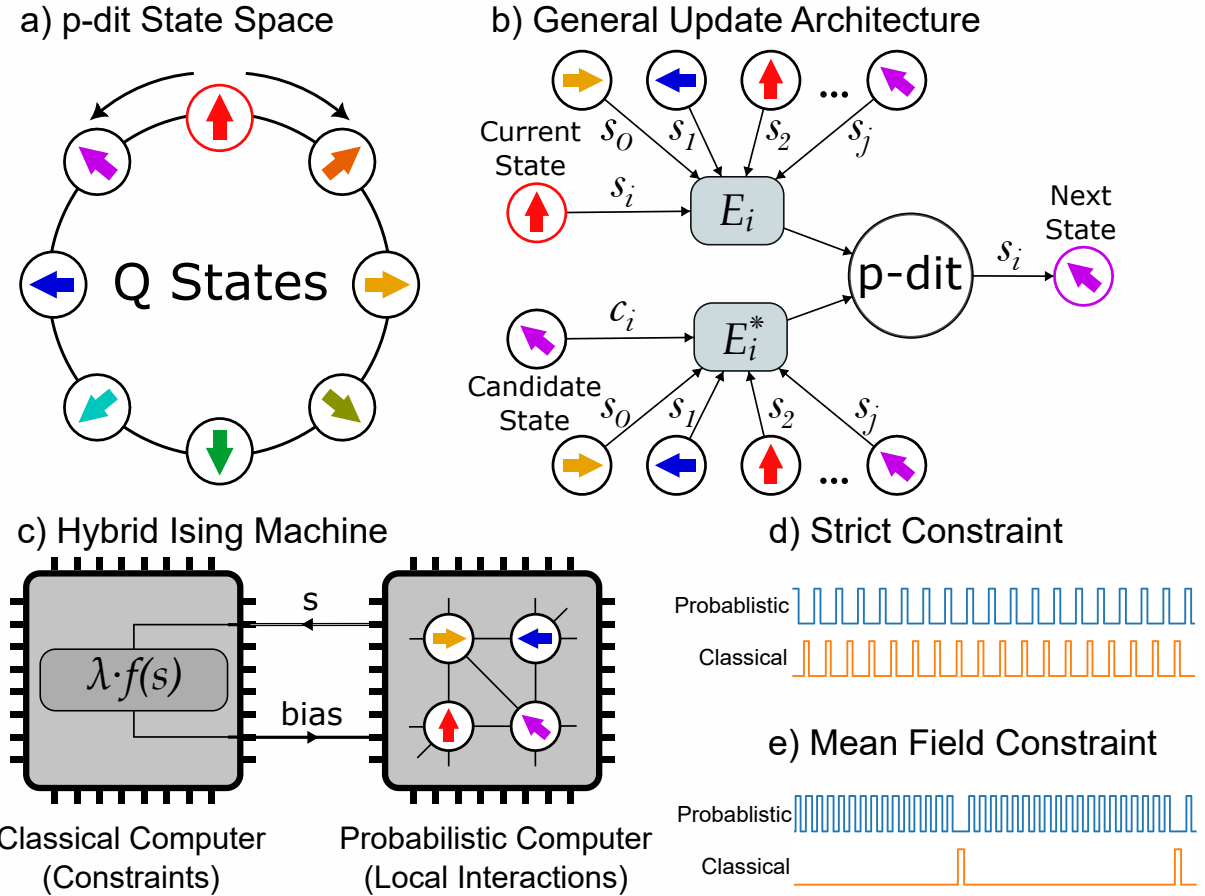


FIG. 1. Overview of the hybrid probabilistic-classical framework. (a) p-bit state space: A p-bit occupies one of Q discrete states arranged on a ring and proposes transitions only to neighboring states. (b) Update rule: The p-bit computes the local energy of its current state (E_i) and a candidate neighbor (E_i^*), then transitions probabilistically based on the difference. (c) Hybrid architecture: The probabilistic subsystem handles local interactions. A classical process computes global constraints and broadcasts a bias signal. Both may reside on the same physical fabric, the separation is conceptual. (d) Strict constraints require the classical process to update at every p-bit flip, imposing high synchronization overhead. (e) Mean-field constraints approximate the constraint as a slowly varying field, allowing updates only once per sweep and reducing classical workload while guiding the system toward feasibility.

Many optimization problems involve variables with more than two states (e.g., coloring, partitioning) that map directly onto Potts spins. Encoding such problems in binary requires multiple coupled bits per variable, expanding the state space to include infeasible configurations that must be suppressed through penalties [8]. Native Potts encodings avoid this overhead entirely, as recent work has shown that eliminating infeasible states alone can accelerate convergence by orders of magnitude [15]. Potts-based hardware has been demonstrated on CMOS-compatible architectures [16], coupled ring-oscillator machines [17], coherent optical implementations [18], and p-bit formulations [9].

In this work, we introduce a hardware-aware p-bit update rule based on local energy comparisons between neighboring Potts states, applicable to general Potts Hamiltonians and validated through finite-size scaling of the 2D Potts model. Fig. 1a and 1b illustrate the p-bit

state space and update structure. For global constraints that cannot be absorbed locally, we introduce mean-field constraints (Figs. 1c–e). Throughout this work, formulations in which such constraints are evaluated exactly are referred to as *strictly constrained* and serve as baselines.

The p-bit is directly inspired by the probabilistic bit (p-bit) [10, 19] and can be viewed as its multi-state generalization. In the p-bit framework, each binary variable stochastically updates based on a local interaction field $I_i = \sum_j J_{ij} m_j + h_i$, which corresponds to the energy difference between the two spin states. The probability of being +1 is

$$p[m_i = +1] = \sigma(2\beta I_i), \quad (2)$$

where $\sigma(\cdot)$ is the sigmoid function, and β is the inverse temperature.

The p-bit extends this to multi-state variables by replacing binary flips with pairwise comparisons. Each

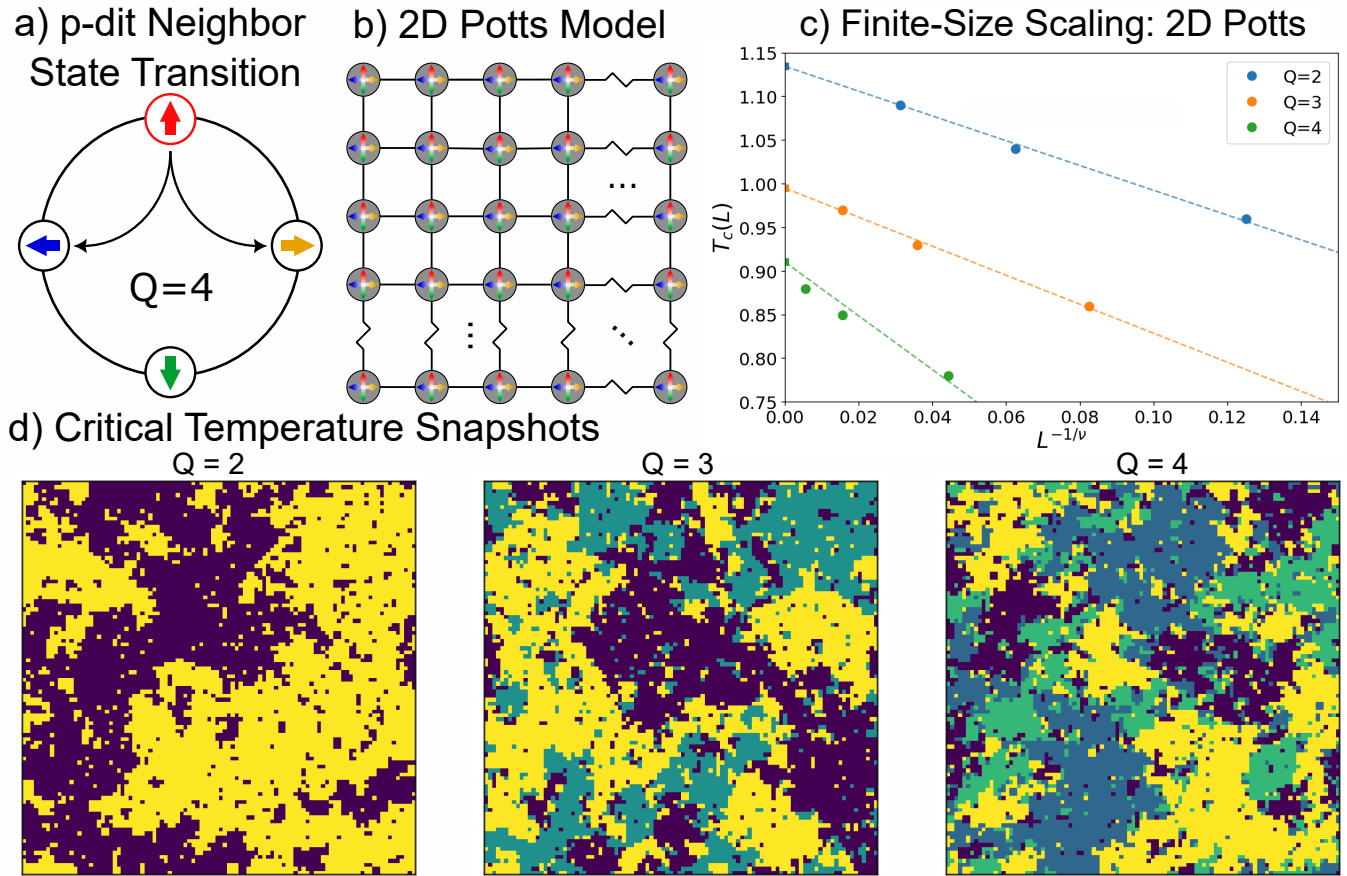


FIG. 2. **Verification of p-bit dynamics using the 2D Potts model.** (a) Four-state p-bit showing discrete angular states and allowed transitions between nearest neighbors. (b) 2D Potts lattice used for validation: $L \times L$ square lattice with nearest-neighbor interactions. (c) Finite-size scaling: Measured critical temperatures $T_c(L)$ for $Q = 2, 3, 4$ follow $T_c(L) \approx T_c(\infty) + aL^{-1/\nu}$ [11–13], consistent with known 2D Potts behavior. (d) Configurations at criticality: Representative $L = 100$ configurations for $Q = 2, 3, 4$ at the fitted critical temperatures.

node maintains a current state s_i and evaluates a candidate state c_i . The energy difference is

$$E(s_i \rightarrow c_i) = \sum_j J_{ij}(s_i \rightarrow c_i, s_j) + h_i(s_i \rightarrow c_i), \quad (3)$$

where $f(x \rightarrow y) \equiv f(x) - f(y)$. Only the local energy difference need be evaluated. The candidate is accepted with probability

$$p[s_i = c_i] = \sigma(\beta E(s_i \rightarrow c_i)). \quad (4)$$

Each update consists of candidate selection followed by stochastic acceptance. We employ nearest-neighbor selection on a circular Potts state space (Fig. 2a): the candidate is chosen uniformly from the two adjacent states. This ensures symmetric proposals while minimizing control complexity. Restricting candidates to neighbors slows mixing but greatly simplifies hardware. Crucially, equilibrium correctness is preserved: the dynamics satisfy detailed balance and converge to the Boltzmann distribution (Sec. VII A).

To validate statistical correctness, we performed finite-size scaling of the 2D ferromagnetic Potts model on $L \times L$ lattices for $L \in \{8, 16, 32\}$ and $Q \in \{2, 3, 4\}$ (Fig. 2b). The extracted critical temperatures follow $T_c(L) \approx T_c(\infty) + aL^{-1/\nu}$ [11–13], with strong agreement to exact values (Fig. 2c). Representative configurations at criticality exhibit the expected domain structure (Fig. 2d). These results establish the p-bit as a statistically correct, hardware-efficient primitive for multi-state probabilistic computing. By embedding constraints into node state spaces and using sequential two-state comparisons, p-dits restore sparsity without sacrificing equilibrium correctness.

While p-dits eliminate constraint-induced density at the node level, many problems impose global constraints that cannot be encoded locally. Addressing these without reintroducing dense couplings motivates the mean-field approach introduced next.

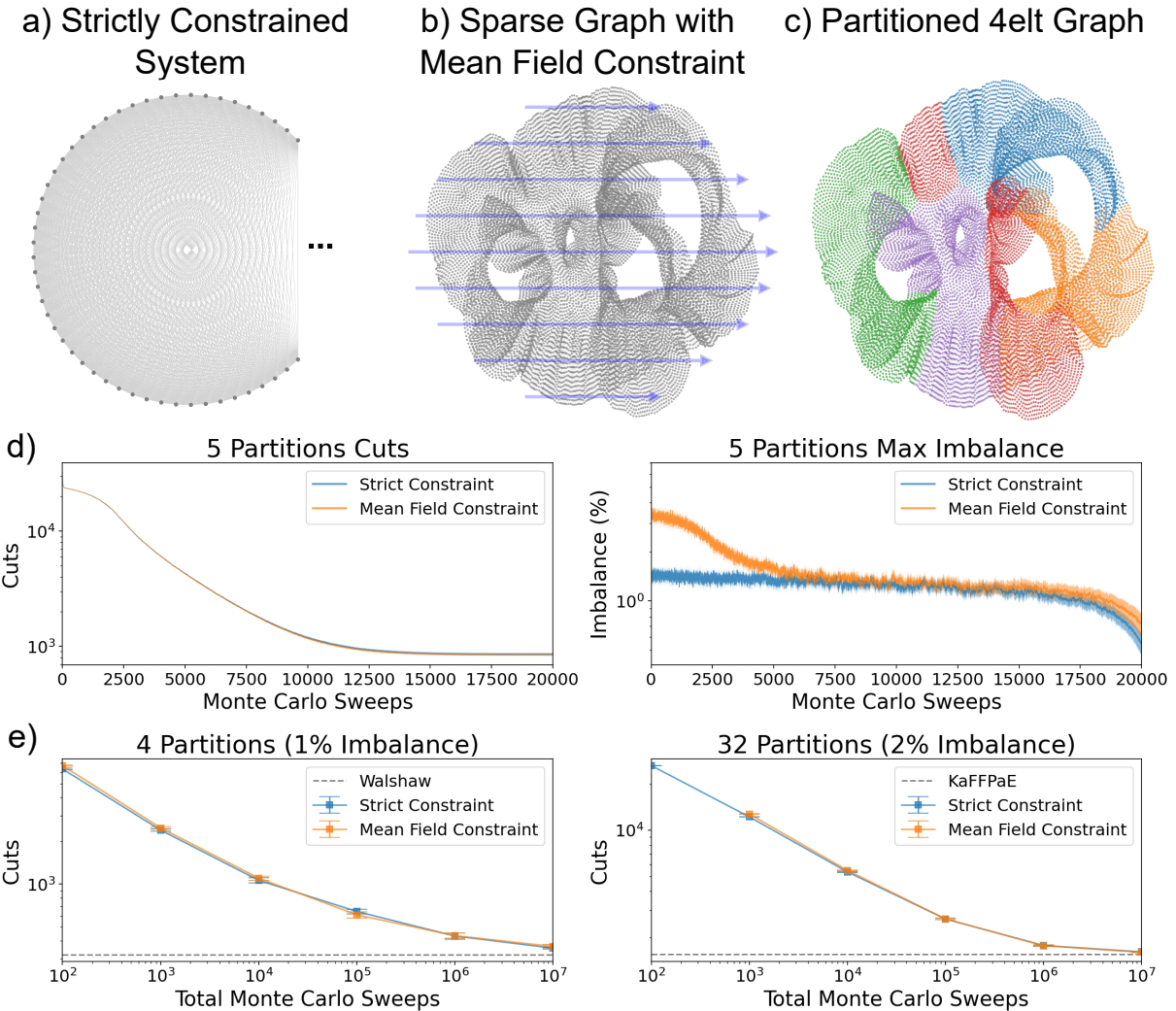


FIG. 3. **Mean-field constraints for balanced minimum-cut partitioning.** (a) Strictly constrained system: The 4elt mesh encoded with all-to-all constraint couplings. (b) Mean-field formulation: The same problem with dense constraint couplings replaced by a global bias signal (blue arrows). (c) Example result: A 5-way partition of 4elt after 10^6 Monte Carlo sweeps. (d) Dynamics: Evolution of cut size and partition imbalance for strict vs. mean-field constraints, averaged over 100 simulated annealing trials. (e) Benchmarking: Solution quality for 4-way (1% maximum imbalance) and 32-way (2% maximum imbalance) partitions. Dashed lines show reference solutions (Walshaw for 4-way; KaFFPaE for 32-way).

III. RESTORING SPARSITY USING MEAN-FIELD CONSTRAINTS

Many optimization problems impose constraints that depend on global properties of the system [8]. Because these constraints act collectively, they cannot be absorbed into local state spaces. When enforced strictly, such global constraints introduce dense or all-to-all interactions, destroying sparsity and limiting parallelism [4, 5].

Mean-field constraints provide a relaxed alternative: rather than coupling nodes through pairwise constraint terms, the constraint influence is approximated by a shared bias updated from the aggregate system state. This replaces constraint-induced density with a single

global signal while retaining a guiding force toward feasibility (Figs. 3a–b). Classical mean-field approximations are well established in statistical physics but can exhibit oscillatory or unstable behavior in strongly constrained systems [20, 21]. Stabilizing these dynamics for hardware implementation requires additional care. We adopt a hybrid architecture combining probabilistic and classical computation (Fig. 1c). The probabilistic subsystem performs local stochastic updates on the sparse interaction graph. A classical subsystem monitors the global state, evaluates constraint violations, and broadcasts a mean-field bias to all nodes. The bias is updated once per Monte Carlo sweep rather than at every node update. While this decoupling restores sparsity, directly applying a sweep-level bias can cause oscillations as the constraint

response overcorrects.

To address this, we interpret the system through a control-theoretic lens: the probabilistic subsystem is the plant, and the classical subsystem is a feedback controller [22]. The constraint violation serves as an error signal, and the mean-field bias is the control input. A simple low-pass filter stabilizes the dynamics:

$$h_{MFC} = \lambda f(\hat{\varepsilon}), \quad \hat{\varepsilon} = \alpha \varepsilon + (1 - \alpha) \hat{\varepsilon}, \quad (5)$$

where ε is the instantaneous constraint error, λ controls constraint strength, and α sets the filter rate. This suppresses rapid fluctuations while maintaining a consistent bias toward feasibility.

The mechanism generalizes readily. Multiple independent mean-field constraints can be enforced simultaneously, and locally dense constraints on node clusters can also be approximated using shared biases. For p-dits, the scalar bias extends to a vector over the state space [14, 20]. Each component corresponds to the energy bias for a particular state, and the contribution enters additively into the local energy difference during updates.

IV. GRAPH PARTITIONING

The graph partitioning problem seeks to divide vertices into multiple communities while minimizing edges crossing between them and maintaining approximately equal-sized partitions [23, 24]. This problem provides a representative test case for constrained optimization, where a sparse objective (cut minimization) is combined with a global constraint (balance).

In the Potts formulation, the Hamiltonian is

$$H = H_{\min} + \lambda H_{\text{bal}}, \quad (6)$$

where H_{\min} encodes the cut objective and H_{bal} enforces balance, with an adjustable constraint parameter λ . The minimum-cut term rewards neighboring vertices in the same partition:

$$H_{\min} = - \sum_{i < j} J_{ij} \delta(s_i, s_j), \quad (7)$$

where J_{ij} is the adjacency matrix and $\delta(\cdot, \cdot)$ is the Kronecker delta. This term is sparse whenever the underlying graph is sparse. Without a balancing constraint, minimizing H_{\min} alone yields a trivial solution where all vertices collapse into one partition. The balancing term penalizes deviations from equal sizes:

$$H_{\text{bal}} = \sum_{k=0}^{Q-1} \left(\sum_i \delta(s_i, k) - \frac{N}{Q} \right)^2, \quad (8)$$

where Q is the number of partitions and N the number of vertices. This term couples all vertices in each partition, inducing dense all-to-all interactions [8].

Using p-dits, partition assignments are encoded directly as multi-state variables. Strict enforcement of H_{bal} preserves correctness but requires sequential updates, negating parallelism. Under mean-field relaxation, the dense balancing edges are replaced by a bias vector reflecting global imbalance. The constraint violation for each partition is

$$\varepsilon_k = \sum_i \delta(s_i, k) - \frac{N}{Q}, \quad (9)$$

filtered according to Eq. (5), yielding

$$h_{MFC} = \lambda \hat{\varepsilon}^2. \quad (10)$$

To evaluate MFC effectiveness, we compared strict and mean-field enforcement on the `4elt` benchmark graph [25] (Fig. 3c). Simulated annealing with 100 independent trials showed comparable cut quality between methods, with MFC exhibiting initially larger imbalance that rapidly converges (Fig. 3d). Both methods improve with additional sweeps, approaching reference solutions from state-of-the-art solvers [25, 26] (Fig. 3e). For 32-way partitioning, an early Monte Carlo sweep data point for MFC is missing because the 2% imbalance threshold could not be maintained, highlighting that MFC requires more sweeps for its low-pass filtering to become effective.

V. HARDWARE IMPLEMENTATION AND PERFORMANCE

Mean-field constraints trade exact Boltzmann dynamics [21] for scalable execution on parallel hardware. The preceding results were obtained on CPU. Here we demonstrate the practical advantage on an FPGA.

We implement a $10 \times 10 \times 10$ cubic graph partitioned into three balanced groups (Fig. 4). Both CPU and FPGA use identical p-bit dynamics, so differences arise primarily from the constraint mechanism and its hardware interaction. Architecture details appear in Sec. VII D.

Figure 4 compares convergence and wall-clock runtime for CPU-based strict constraints, CPU-based MFC, and FPGA-based MFC. All implementations converge toward similar cut values, consistent with KaFFPaE reference solutions [26]. On CPU, runtime differences between strict and MFC are modest since updates run sequentially regardless. On FPGA, MFC enables parallel updates on the sparse graph, yielding nearly two orders of magnitude speedup when communication overhead is excluded.

The FPGA runtime scales linearly with sweep count and matches predicted clock-cycle timing. Reported results include approximately ten seconds of host-device communication overhead per run because the annealing schedule runs on the host. This overhead could be eliminated by on-chip annealing. A strict-constraint FPGA implementation was not pursued because exact balancing

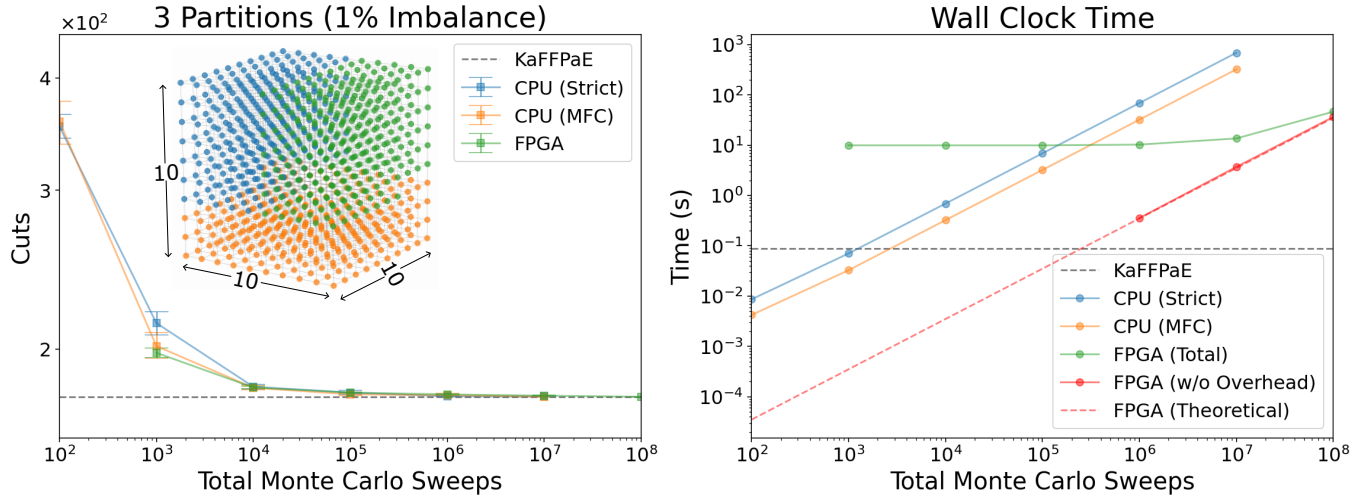


FIG. 4. **Hardware performance for balanced min-cut partitioning.** Left: Cut-quality convergence for strict constraints, MFC, and FPGA-MFC on a $10 \times 10 \times 10$ cube partitioned into three groups (1% maximum imbalance). All approaches converge toward the KaFFPaE reference. Right: Wall-clock runtime vs. Monte Carlo sweeps. FPGA results shown with and without host-device overhead. The FPGA exhibits linear scaling, approaching one p-bit update per clock cycle.

would reintroduce dense interactions, requiring sequential updates and negating hardware parallelism [5, 8].

These results confirm that mean-field constraints are central to scalable hardware acceleration. By restoring sparsity without sacrificing solution quality, MFC allows p-bit solvers to recover performance traditionally associated with sparse Ising machines, even for globally constrained problems.

VI. DISCUSSION

Mean-field constraints provide an effective mechanism for restoring sparsity, but they are inherently approximate. MFC does not preserve the exact constrained energy landscape and therefore does not guarantee correct Boltzmann sampling [21]. As a result, mean-field constraints are best suited for optimization rather than applications requiring faithful equilibrium sampling.

Because constraint feedback is applied at the sweep level rather than instantaneously, the dynamics form a delayed feedback loop. Large gain values (λ) or fast update rates (α) can cause oscillatory behavior as the system overcorrects [22]. Stabilizing the dynamics requires careful hyperparameter selection and may limit how tightly constraints can be enforced. Problems requiring strict satisfaction of hard constraints with very tight tolerances may not be well suited to a purely mean-field formulation. A two-stage strategy may offer the best of both approaches: use MFC to quickly reach a feasible region, then refine with strict enforcement.

This work introduces two complementary mechanisms for reducing constraint-induced density. p-dits handle local constraints exactly by embedding them into the node state space, preserving the energy landscape while

eliminating infeasible configurations. Mean-field constraints handle global constraints approximately through shared feedback signals, restoring sparsity at the cost of exact fidelity. Together, these techniques allow constrained problems to be decomposed according to constraint structure and addressed with the appropriate strategy.

Restoring sparsity has direct impact on hardware efficiency. The FPGA results demonstrate that MFC, combined with p-bit dynamics, enables orders-of-magnitude speedups over CPU implementations while maintaining solution quality. Although demonstrated on an FPGA, the principles apply broadly to GPUs, ASICs, and emerging probabilistic substrates.

Several directions follow naturally: more sophisticated feedback controllers (adaptive or learned), systems with multiple interacting constraints combining strict and relaxed enforcement, and integration with other sparsification techniques to expand the class of problems addressable on probabilistic hardware.

While constraints add density to graphs, not all underlying unconstrained graphs are inherently sparse. Therefore, another promising direction is generalizing MFC techniques to relax specific graph nodes that have high edge density as a means to sparsify base graphs.

VII. METHODS

A. Detailed Balance

To establish that the p-bit update rule with nearest-neighbor candidate selection samples from the correct stationary distribution, we verify that the resulting Markov chain satisfies detailed balance. Detailed balance

requires that, for any two states i and j ,

$$\pi_i P_{ij} = \pi_j P_{ji},$$

where π_i denotes the stationary probability of state i and P_{ij} is the transition probability from i to j .

Under the nearest-neighbor candidate selection scheme, transitions are allowed only between adjacent states on the Potts ring. The transition probability can therefore be written as

$$P_{ij} = \begin{cases} A_{ij}/2, & j = (i \pm 1) \bmod Q, \\ 0, & \text{otherwise,} \end{cases}$$

where the factor of $1/2$ accounts for uniform selection between the two neighboring candidates and A_{ij} is the acceptance probability defined in Eq. (4),

$$A_{ij} = \sigma(\beta E(i \rightarrow j)).$$

Substituting this transition probability into the detailed balance condition yields

$$\frac{\pi_j}{\pi_i} = \frac{A_{ij}}{A_{ji}} = \exp(-\beta [E_j - E_i]),$$

which implies that the stationary distribution satisfies

$$\pi_i \propto \exp(-\beta E_i).$$

Since this relation holds for any pair of neighboring states, it extends recursively to all states in the ring. The p-bit dynamics therefore satisfy detailed balance and converge to the Boltzmann distribution.

While this work focuses on nearest-neighbor candidate selection for hardware efficiency, the above argument generalizes to a broader class of proposal mechanisms. Any candidate selection scheme that is probabilistic, ergodic, symmetric, and excludes self-transitions will satisfy detailed balance when combined with the acceptance rule in Eq. (4). Different proposal mechanisms trade off mixing speed against implementation complexity.

B. p-bit Validation

To validate the statistical correctness of the p-bit update rule, we measured the finite-size critical temperatures $T_c(L)$ of the two-dimensional ferromagnetic q -state Potts model using p-bit Monte Carlo dynamics. The model is defined by the Hamiltonian

$$H = - \sum_{\langle i,j \rangle} \delta(s_i, s_j),$$

on an $L \times L$ square lattice with nearest-neighbor interactions. Open boundary conditions were used in all simulations.

1. Determination of $T_c(L)$

To obtain $T_c(L)$, the system was simulated across inverse temperatures $\beta \in [0.1, 2.0]$ in steps of 0.01. For each (L, q, β) configuration, ten independent trials were performed, each consisting of 10^6 p-bit updates per spin, following standard Monte Carlo sampling procedures [27].

The magnetization was measured as a function of β , and the critical point for each trial was identified as the location of the maximum derivative of the magnetization curve. These values were averaged across trials to obtain the reported $T_c(L)$, which were subsequently used for the finite-size scaling fits in Fig. 2c.

2. Finite-Size Scaling Fit

The critical temperatures in the thermodynamic limit are known exactly from Baxter's solution of the two-dimensional Potts model [28, 29],

$$T_c(\infty) = \frac{1}{\ln(1 + \sqrt{q})}.$$

The corresponding correlation-length critical exponents for the $q = 2, 3, 4$ universality classes are also known exactly [14, 30],

$$\nu = 1, \quad \nu = \frac{5}{6}, \quad \nu = \frac{2}{3}.$$

Using these known quantities, the measured critical temperatures were fitted to the finite-size scaling form

$$T_c(L) \approx T_c(\infty) + aL^{-1/\nu},$$

with a as the single fitting parameter [11–13]. The resulting coefficients were

$$a = -1.420, \quad a = -1.662, \quad a = -3.081$$

for $q = 2, 3, 4$ respectively.

C. CPU Simulations

All CPU-based simulations were implemented in C++ using a Monte Carlo framework that directly simulates p-bit dynamics. Simulations were executed on an AMD Ryzen 7940HS CPU, with strict and mean-field constraint enforcement differing only in the constraint update mechanism.

KaFFPaE runs were executed locally from an open source KaHIP (v3.17) package. Timing reported in Fig. 4 was found using a binary search varying the “time_limit” parameter until a majority of 50 tested seeds reached the 177 cut target. The parameters “k” and “imbalance” were set to 3 and 1.0 respectively. All other parameters were set to their default values.

D. FPGA Implementation

The hybrid Ising machine was implemented on an Alveo U250 FPGA and operated at a clock frequency of 100 MHz. The probabilistic subsystem implements p-dit-based Potts dynamics, while a classical feedback controller computes and applies the mean-field constraint. A host CPU communicates the simulated annealing schedule over PCIe. All experiments reported in Sec. V use three-state p-dits corresponding to the three target partitions.

The probabilistic subsystem and feedback controller are sequentially activated. A full update of both systems takes 37 clock cycles; 2 cycles are allocated to the probabilistic subsystem to update each color group. The remaining 35 cycles are required for a pipelined implementation of the feedback controller meant to maximize the inter-system clock frequency. A majority of this time (32 cycles) is produced by a batched population count; the remaining 3 cycles are attributed to calculating and distributing the new MFC bias.

To reduce computational complexity and maximize throughput, energy differences are evaluated directly rather than computing absolute energies. For each node i , the local energy change associated with a proposed transition $s_i \rightarrow c_i$ is decomposed into a cut term and a balancing term,

$$E_i(s_i \rightarrow c_i) = E_{\min,i}(s_i \rightarrow c_i) + E_{\text{bal},i}(s_i \rightarrow c_i).$$

The cut contribution is computed as

$$E_{\min,i}(s_i \rightarrow c_i) = \sum_{j \in \Omega_i} f(s_i, c_i, s_j),$$

where Ω_i denotes the neighborhood of node i and

$$f(s_i, c_i, s_j) = \begin{cases} -\beta, & s_i = s_j, \\ \beta, & c_i = s_j, \\ 0, & \text{otherwise.} \end{cases}$$

β values are expressed as 10-bit fixed point (Q6.3).

The balancing contribution is computed using filtered population counts,

$$E_{\text{bal},i}(s_i \rightarrow c_i) = \beta \lambda \hat{N}_{s_i} - \beta \lambda \hat{N}_{c_i} - \beta \lambda,$$

where the filtered population vector is updated according to

$$\hat{\mathbf{N}} = \alpha \mathbf{N} + (1 - \alpha) \hat{\mathbf{N}},$$

and \mathbf{N} denotes the instantaneous population count for each state. $\beta \lambda$ terms are precomputed by the CPU and passed as a single value to the FPGA.

This formulation allows both the cut objective and the mean-field balancing constraint to be evaluated using local information and a small number of global registers, avoiding dense pairwise interactions and enabling efficient parallel execution.

DATA AVAILABILITY

The data that support the findings of this article are not publicly available. The data are available from the authors upon reasonable request.

CODE AVAILABILITY

The computer code used in this study is available from the corresponding author upon reasonable request.

AUTHOR CONTRIBUTIONS

KC-C and KYC conceived the study and wrote the manuscript. KYC supervised the study. KC-C conducted experiments regarding p-dit verification, MFC scaling on FPGA and CPU, and developed FPGA structure. KL introduced the minimum-cut formulation for p-dits and supervised CPU testing. KJ conducted strict constraint and MFC testing and benchmarking for CPU study. All authors reviewed the manuscript.

COMPETING INTERESTS

The authors declare no competing interests.

ACKNOWLEDGMENTS

This material is based upon work supported by, or in part by, the Army Research Laboratory under grant number W911NF-24-1-0228. Thanks to Christian Duffee and Pedram Khalili Amiri for fruitful discussions regarding ASIC implementations.

[1] Naeimeh Mohseni, Peter L. McMahon, and Tim Byrnes. Ising machines as hardware solvers of combinatorial optimization problems. *Nature Reviews Physics*, 4(6):363–379, Jun 2022.

[2] Masoud Mohseni, Artur Scherer, K Grace Johnson, Oded Wertheim, Matthew Otten, Navid Anjum Aadir, Yuri Alexeev, Kirk M Bresniker, Kerem Y Camsari, Barbara Chapman, et al. How to build a quantum supercom-

- puter: Scaling from hundreds to millions of qubits. *arXiv preprint arXiv:2411.10406*, 2024.
- [3] Y Fu and P W Anderson. Application of statistical mechanics to np-complete problems in combinatorial optimisation. *Journal of Physics A: Mathematical and General*, 19(9):1605, jun 1986.
- [4] Navid Anjum Aadit, Andrea Grimaldi, Mario Carpenteri, Luke Theogarajan, John M. Martinis, Giovanni Finocchio, and Kerem Y. Camsari. Massively parallel probabilistic computing with sparse ising machines. *Nature Electronics*, 5(7):460–468, June 2022.
- [5] M. Mahmudul Hasan Sajeeb, Navid Anjum Aadit, Shuvro Chowdhury, Tong Wu, Cesely Smith, Dhruv Chinmay, Atharva Raut, Kerem Y. Camsari, Corentin Delacour, and Tathagata Srimani. Scalable connectivity for ising machines: Dense to sparse. *Physical Review Applied*, 24(1), July 2025.
- [6] Jeffrey Chou, Suraj Bramhavar, Siddhartha Ghosh, and William Herzog. Analog coupled oscillator based weighted ising machine. *Scientific Reports*, 9(1):14786, Oct 2019.
- [7] Nihal Sanjay Singh, Keito Kobayashi, Qixuan Cao, Kenal Selcuk, Tianrui Hu, Shaila Niazi, Navid Anjum Aadit, Shun Kanai, Hideo Ohno, Shunsuke Fukami, and Kerem Y. Camsari. Cmos plus stochastic nanomagnets enabling heterogeneous computers for probabilistic inference and learning. *Nature Communications*, 15(1):2685, Mar 2024.
- [8] Andrew Lucas. Ising formulations of many np problems. *Frontiers in Physics*, 2, 2014.
- [9] Christian Duffee, Jordan Athas, Andrea Grimaldi, Deborah Volpe, Giovanni Finocchio, Ermin Wei, and Pedram Khalili Amiri. P-dits: Probabilistic d-dimensional bits for extended-variable probabilistic computing. *Physical Review Applied*, 24(4):044077, 2025.
- [10] Jan Kaiser and Supriyo Datta. Probabilistic computing with p-bits. *Applied Physics Letters*, 119(15), October 2021.
- [11] Michael E. Fisher and Michael N. Barber. Scaling theory for finite-size effects in the critical region. *Phys. Rev. Lett.*, 28:1516–1519, Jun 1972.
- [12] Vladimir Privman and Michael E. Fisher. Universal critical amplitudes in finite-size scaling. *Phys. Rev. B*, 30: 322–327, Jul 1984.
- [13] K. Binder and D. P. Landau. Finite-size scaling at first-order phase transitions. *Phys. Rev. B*, 30:1477–1485, Aug 1984.
- [14] Fa-Yueh Wu. The potts model. *Reviews of Modern Physics*, 54(1):235, 1982.
- [15] Devrath Iyer and Sara Achour. Efficient optimization with encoded ising models. In *2025 IEEE International Symposium on High Performance Computer Architecture (HPCA)*, pages 85–98. IEEE, 2025.
- [16] William Whitehead, Zachary Nelson, Kerem Y Camsari, and Luke Theogarajan. CMOS-compatible Ising and Potts annealing using single-photon avalanche diodes. *Nature Electronics*, 6:1009–1019, 2023.
- [17] Yilmaz Ege Gonul and Baris Taskin. Multi-phase coupled CMOS ring oscillator based Potts machine. In *Proceedings of the 43rd IEEE/ACM International Conference on Computer-Aided Design (ICCAD)*, 2024.
- [18] Kyo Inoue, Kazuhiro Yoshida, and Shogo Kitahara. Coherent Potts machine based on an optical loop with a multilevel phase-sensitive amplifier. *Optics Communications*, 522:128639, 2022.
- [19] Kerem Yunus Camsari, Rafatul Faria, Brian M. Sutton, and Supriyo Datta. Stochastic-bits for invertible logic. *Physical Review X*, 7(3), July 2017.
- [20] Anirban Basak and Sumit Mukherjee. Universality of the mean-field for the potts model. *arXiv preprint arXiv:1508.03949*, 2016.
- [21] Vishesh Jain, Frederic Koehler, and Elchanan Mossel. The mean-field approximation: Information inequalities, algorithms, and complexity. *arXiv preprint arXiv:1802.06126*, 2018.
- [22] Karl Johan Åström and Richard M. Murray. *Feedback Systems: An Introduction for Scientists and Engineers*. Princeton University Press, 2006.
- [23] George Karypis and Vipin Kumar. A fast and high quality multilevel scheme for partitioning irregular graphs. *SIAM Journal on Scientific Computing*, 20(1):359–392, 1998.
- [24] Aydin Buluc, Henning Meyerhenke, Ilya Safro, Peter Sanders, and Christian Schulz. Recent advances in graph partitioning. *arXiv preprint arXiv:1311.3144*, 2015.
- [25] Chris Walshaw. The graph partitioning archive, 2024.
- [26] Peter Sanders and Christian Schulz. Distributed evolutionary graph partitioning. *arXiv preprint arXiv:1110.0477*, 2011.
- [27] M.E.J. Newman and G.T. Barkema. *Monte Carlo Methods in Statistical Physics*. Oxford University Press, 1999.
- [28] Rodney J. Baxter. Potts model at the critical temperature. *Journal of Physics C: Solid State Physics*, 6(23): L445, 1973.
- [29] Rodney J. Baxter. *Exactly Solved Models in Statistical Mechanics*. Academic Press, 1982.
- [30] Bernard Nienhuis. Critical behavior of two-dimensional spin models and charge asymmetry in the coulomb gas. *Journal of Statistical Physics*, 34(5):731–761, Mar 1984.